Polarization-Controlled Tunable Directional Coupling of Surface Plasmon Polaritons

Jiao Lin *et al.*

Science **340**, 331 (2013);
DOI: 10.1126/science.1233746

Science (print ISSN 0036-8075; online ISSN 1095-9203) is published weekly, except the last week in December, by the American Association for the Advancement of Science, 1200 New York Avenue NW, Washington, DC 20005.

Polarization-Controlled Tunable Directional Coupling of Surface Plasmon Polaritons

Jiao Lin,[1,2]* J. P. Balthasar Mueller,[1]* Qian Wang,[3] Guanghui Yuan,[3] Nicholas Antoniou,[4] Xiao-Cong Yuan,[5] Federico Capasso[1]†

Light can be coupled into propagating electromagnetic surface waves at a metal-dielectric interface known as surface plasmon polaritons (SPPs). This process has traditionally faced challenges in the polarization sensitivity of the coupling efficiency and in controlling the directionality of the SPPs. We designed and demonstrated plasmonic couplers that overcome these limits using polarization-sensitive apertures in a gold film. Our devices enable polarization-controlled tunable directional coupling with polarization-invariant total conversion efficiency and preserve the incident polarization information. Both bidirectional and unidirectional launching of SPPs are demonstrated. The design is further applied to circular structures that create radially convergent and divergent SPPs, illustrating that this concept can be extended to a broad range of applications.

Surface plasmon polaritons (SPPs) are propagating excitations that arise from the coupling of light with collective oscillations of the electrons at the surface of a metal (*1*). The strong dependence of their properties on the composition and structure of the surface has led to many advances in the control of light at the nanoscale (*2*–*9*), holding promise for optical information technology and optoelectronics (*10*, *11*) and for the study and engineering of light-matter interaction (*12*, *13*).

The polarization states of the optical signal that can be coupled to a plasmonic device are often limited by the selectivity of the coupling process. For directional SPP excitation, usually only the component of the incident light that is polarized perpendicularly to either groove- or ridge-like scattering elements (in the case of gratings) or to the metal surface itself (in the case of prism-based schemes) can be coupled into SPPs (*1*). Light in the orthogonal polarization does not couple to SPPs, leading to a decrease in the SPP signal and a loss of information about the incident polarization state.

Additional challenges arise in controlling the direction of propagation of the generated SPPs. Poor directionality frequently represents a substantial source of noise and reduces efficiency. This has lead to the development of several schemes that couple unidirectionally, albeit with limited dynamic tunability (*14*–*16*).

We present a directional plasmonic coupler that addresses these challenges by offering polarization-invariant coupling efficiency to SPPs while allowing full control over the distribution of power between two counter-propagating SPP modes. This includes unidirectional coupling and preserves polarization information.

A narrow aperture in a metal film selectively scatters incident light that is polarized perpendicular to it, giving rise to SPPs. This occurs both for light incident on the front and for light incident on the back of apertures that fully perforate the film. In the latter case, SPPs are transmitted through the apertures to the other side of the film, where they are launched across the surface. The SPP emission pattern of a subwavelength aperture is approximately that of an in-plane dipole (*17*), which is known analytically (*18*) and plotted in Fig. 1A along with the corresponding orientation of the aperture. When many such dipoles are arranged in a column with a spacing that is smaller than the SPP wavelength (λ_{SPP}), the launched SPPs are plane waves that propagate perpendicularly away toward either side of the column (Fig. 1B). This effect is independent of the orientation of the dipoles of the column. We can therefore create a source of SPP plane waves propagating in a fixed direction that can be designed to selectively respond to a polarization component of the incident light determined by the orientation of the apertures of the column.

A more complex polarization response can be achieved by fabricating multiple columns on the metal surface, resulting in interference of the SPP waves created by individual columns. We consider two parallel columns (Fig. 1C) that are spaced a distance S apart and are made up of apertures with width W and length L, such that $W << L < \lambda_{SPP}$. The apertures of one column are spaced a distance D apart, with $D < \lambda_{SPP}$. The columns are offset by half a period (D/2) along their axes to reduce near-field coupling and scattering of the SPPs by neighboring apertures. With this geometry, simulations showed both effects to be negligible (*19*). The apertures of the first and second column are oriented at angles θ_1 and θ_2 with respect to the y axis. If light with an electric field $\vec{E}$ is normally incident on the metal surface, the respective columns will then couple to the components of the incident field $\vec{E}_1$ and $\vec{E}_2$ that are polarized at angles $90° + \theta_1$ and $90° + \theta_2$. The conversion efficiency C_i of a column scales as $C_i \propto \cos^2 \theta_i$ because the SPP emission pattern of the individual apertures is anisotropic (Fig. 1A) and only the component of the wave that is launched perpendicular to the column is not cancelled by the fields of the surrounding dipoles (Fig. 1B).

The field components $\vec{E}_1$ and $\vec{E}_2$ can have a relative phase δ that is preserved by the coupling process and transferred to the SPPs. If the propagation loss of the SPPs over the small distance S is neglected, interference of the SPP waves launched by each column results in time-averaged SPP field intensities propagating to the right (I_R) and the left (I_L) to the pair of columns (*19*):

$$I_R \propto [(C_1E_1^2 + C_2E_2^2) + 2E_1E_2\cos(k_{SPP}S + \delta)]$$
$$I_L \propto [(C_1E_1^2 + C_2E_2^2) + 2E_1E_2\cos(k_{SPP}S - \delta)] \quad (1)$$

where the intensities are calculated in the dielectric. E_1 and E_2 denote the amplitudes of the field components coupled to the respective columns and $k_{SPP} = \frac{2\pi}{\lambda_{SPP}}$ the SPP wave number. If $|\theta_1 - \theta_2| = 90°$, then $|\vec{E}|^2 = |\vec{E}_1|^2 + |\vec{E}_2|^2$. We make the particular choice of $\theta_1 = 45°$ and $\theta_2 = 45° + 90° = 135°$, in which case the coupling coefficients of the two columns $C_1 = C_2 = C$. If we adjust the lateral spacing S of the columns with respect to the SPP wavelength to $S = \frac{\pi}{2}k_{SPP}^{-1}$, Eq. 1 becomes

$$I_R \propto C[(E_1^2 + E_2^2) - 2E_1E_2\ \sin\delta]$$
$$I_L \propto C[(E_1^2 + E_2^2) + 2E_1E_2\ \sin\delta] \quad (2)$$

Notably, the combined intensity of the coupled SPP fields $I_R + I_L \propto C|\vec{E}|^2$ is proportional to the intensity of the incident light but is independent of δ and of the relative magnitude of the coupled field components E_1 and E_2. The total power that is converted to SPPs can thus be made independent of the polarization of the incident light. Moreover, the polarization dependence in Eq. 2 can be used to adjust the fraction of the total converted power that is propagating in the SPP waves launched either toward the left or toward the right side of the column pair by changing the polarization state of the incident light. The distribution of the intensities in the counter-propagating SPP modes as a function of polarization as predicted by Eq. 2 is shown in Fig. 2A. Here, we expressed the polarization state of the incident light in complex number representation (*20*) in terms of ψ and δ according to

$$e^{-i\delta}\tan\psi = \frac{E_2^c}{E_1^c} \quad (3)$$

where E_1^c and E_2^c are the complex amplitudes of the field components $\vec{E}_1$ and $\vec{E}_2$, respectively.

[1]School of Engineering and Applied Sciences, Harvard University, Cambridge, MA 02138, USA. [2]Singapore Institute of Manufacturing Technology, 71 Nanyang Drive, Singapore 638075, Singapore. [3]School of Electrical and Electronic Engineering, Nanyang Technological University, Nanyang Avenue, Singapore 639798, Singapore. [4]Center for Nanoscale Systems, Harvard University, Cambridge, MA 02138, USA. [5]Institute of Modern Optics, Key Laboratory of Optical Information Science and Technology, Ministry of Education of China, Nankai University, Tianjin 300071, China.

*These authors contributed equally to this work.
†Corresponding author. E-mail: capasso@seas.harvard.edu

Unidirectional coupling occurs when the incident light is circularly polarized ($E_1 = E_2; \frac{\pi}{2}$), with the direction determined by the handedness. In this way, the two circular polarization states represent two separate channels that can selectively address structures to either side of the coupler. Switchable unidirectional coupling is possible by changing the handedness of the incident light (Fig. 2A). The structure is analogous to a polarizing beam

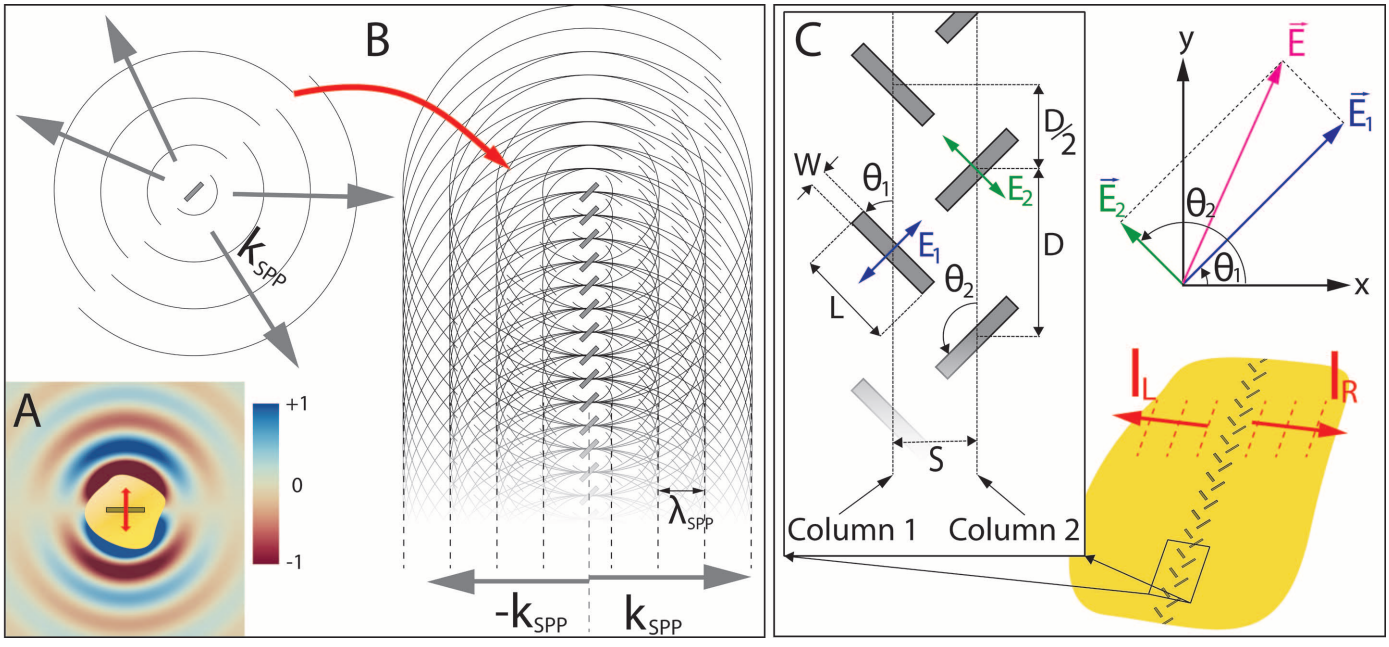

Fig. 1. Closely spaced subwavelength apertures as polarization-selective SPP plane-wave sources. (**A**) The calculated normal component of the SPP electric field launched by an in-plane dipole (in arbitrary units), which is an approximation for a subwavelength aperture in a gold film (overlay) that is scattering incident light polarized perpendicular to its long axis (polarization indicated by a red arrow). (**B**) The SPP waves generated by a single aperture propagate radially away from it, with wavefronts shown in black. The waves emitted from many apertures arranged in a column with subwavelength spacing interfere constructively along planes parallel to the column, shown as dashed lines. SPP wave vectors (k_{SPP}) are shown as gray arrows. (**C**) Two columns of apertures (1 and 2) are positioned in parallel with spacing S. The columns couple to the field components $\vec{E}_1$ (blue arrows) and $\vec{E}_2$ (green arrows) of the incident field $\vec{E}$ (pink arrow). The resulting combined SPP plane waves propagating away from the column pair (red arrows) have intensities I_R and I_L.

Fig. 2. Changing the incident polarization enables continuous tuning of the directionality of the launched SPPs. (**A**) Distribution of power between the SPP waves propagating to either side of the coupler as a function of the polarization state of the normally incident light according to Eq. 2. The incident polarization states are expressed in complex number notation in terms of the angles Ψ and δ (Eq. 3) and additionally shown as a black overlay. (**B**) Multiple parallel column pairs are spaced λ_{SPP} apart. The structure is shown such that right (left) CPL is coupled to the right (left) when it is incident from the top. (**C**) FDTD simulation of the near-field intensity (arbitrary units) above a coupler made up of five column pairs (white overlay) under illumination by incident light with linear and circular polarizations (pink arrows).

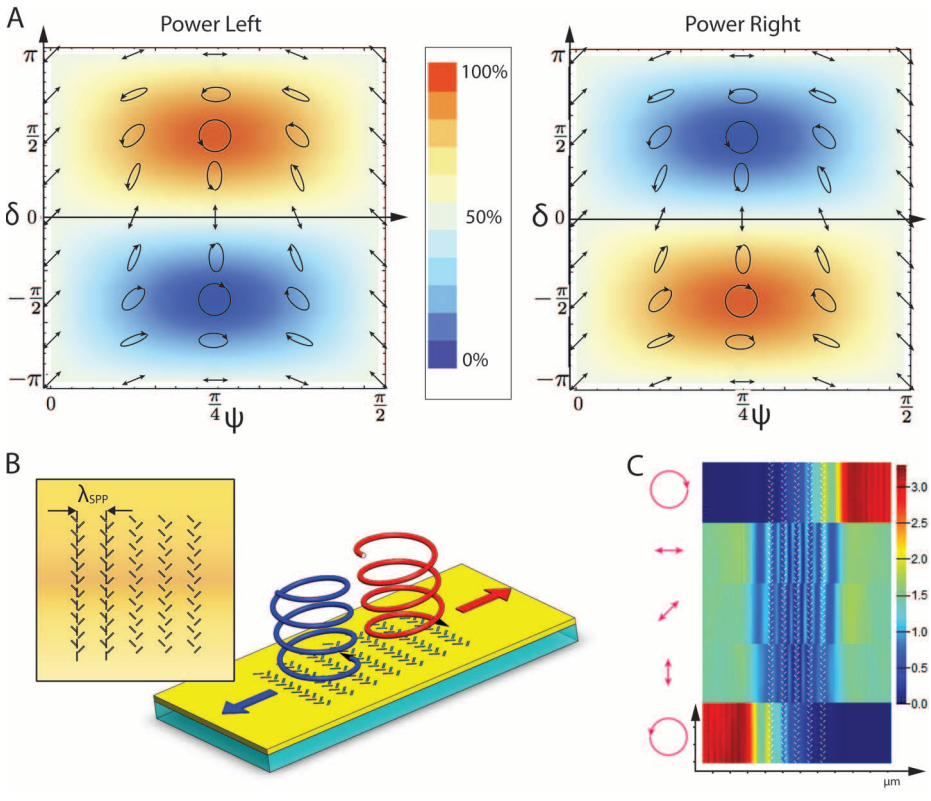

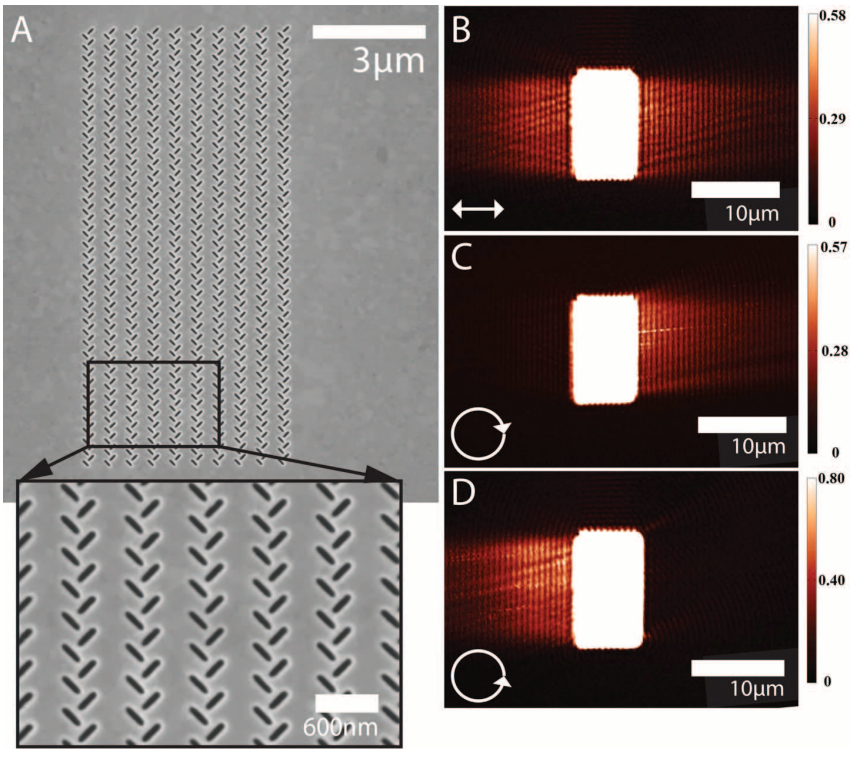

Fig. 3. Measurement of the SPPs launched by a fabricated coupler. (**A**) Scanning electron microscope (SEM) image of a structure fabricated in a gold film for operation at $\lambda = 633$ nm. (**B** to **D**) NSOM images of the structure under illumination from the back by LPL (B), right CPL (C), and left CPL (D). The state of incident polarization is shown by white arrows.

splitter with two SPP output channels because the SPP fields propagating to the left and the right correspond to the circularly polarized components of the incident light. The polarization state of the incident light is then fully encoded in the amplitude and relative phase of the SPPs.

The cross-section of the coupler can be increased by placing several column pairs an SPP wavelength apart in the manner of a second-order grating (Fig. 2B). The side of the structure toward which each circularly polarized state is routed relative to the observer is shown in Fig. 2B.

We performed full-wave finite-difference time-domain (FDTD) simulations of the SPPs created by a group of five column pairs patterned on a gold surface for various incident polarizations. This structure was designed for operation at $\lambda = 633$ nm, corresponding to $\lambda_{SPP} \cong 606$ nm. The geometrical parameters of the structure are $S = 150$ nm, $D = 300$ nm, $W = 40$ nm, and $L = 200$ nm. The column pairs are spaced 600 nm apart, and the thickness of the Au film is 200 nm. The results show good agreement with the predictions of Eq. 2 (Fig. 2C). Further simulation results can be found in (*19*).

We fabricated 10 column pairs, with $S = 150$ nm, $D = 300$ nm, $W = 50$ nm, and $L = 200$ nm in a 150-nm-thick gold film using focused ion beam milling (FIB). The devices were back-illuminated with polarized 633-nm laser light, and the SPPs were measured using near-field

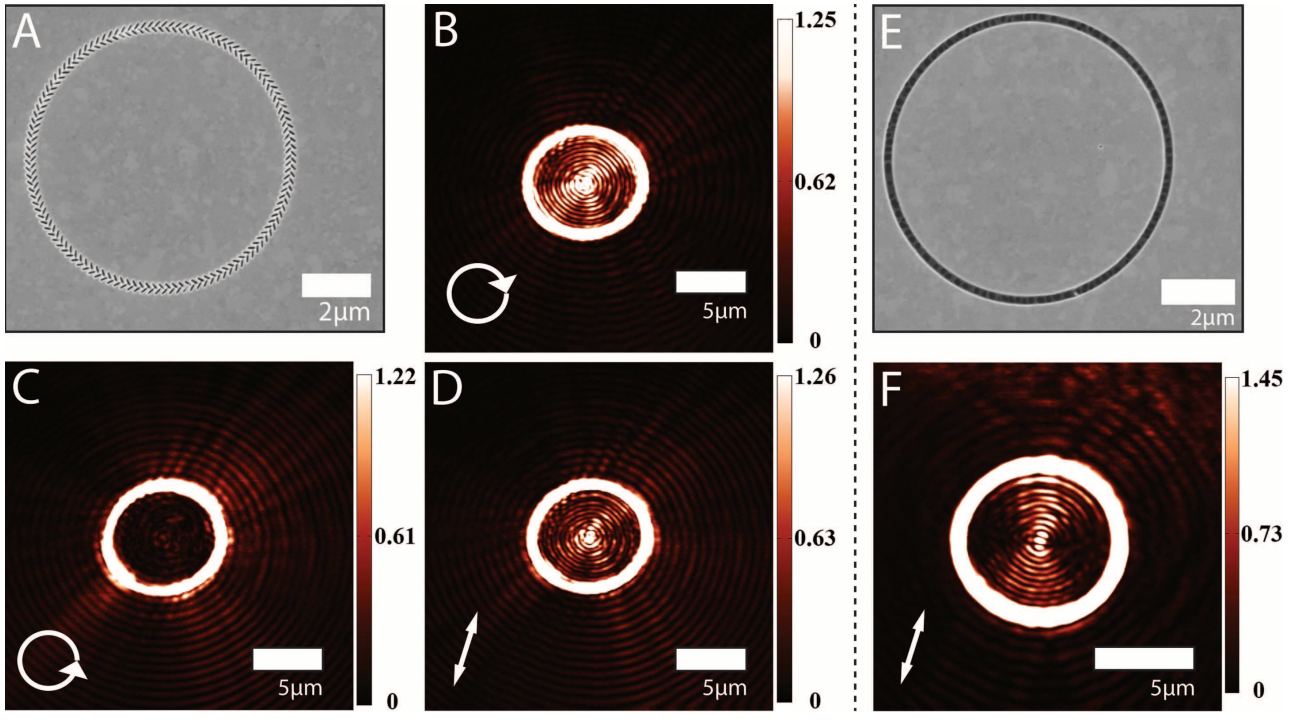

Fig. 4. Curved structures and polarization-invariant coupling efficiency. (**A**) SEM image of a circular coupler based on our design. (**B**) NSOM images of the coupler under right CPL, resulting in radially inward coupling, which creates a high-intensity standing wave within the circle. (**C**) NSOM image under left CPL, resulting in radial unidirectional coupling away from the circle and low intensity within the circle. (**D**) NSOM image of the coupler under LPL, which results in equal power propagating inward and outward. SPPs are generated by sections of the coupler oriented at all angles with respect to the incident polarization. (**E**) SEM image of a circular groove of the same radius, representative of a conventional plasmonic coupler. (**F**) NSOM image of the circular groove under LPL, showing generation of SPPs only where the groove is perpendicular to the incident polarization.

scanning optical microscopy (NSOM) (*19*). The observed field distributions are in good agreement with the theoretical model (Fig. 3). The NSOM micrographs exhibit fringe patterns that result from the interference of the SPPs with incident light directly transmitted through the film, confirming that the measured optical signal corresponds to the near-field (*19*). Figure 3, B to D, shows in particular that circularly polarized light (CPL) of opposite handedness generates counter-propagating SPP beams, whereas linearly polarized light (LPL) launches SPP beams of equal intensity toward either side of the coupler.

This coupling scheme can be generalized by adding curvature to the column pairs on the metal surface. A coupler bent into a circle can be used to achieve radial unidirectional coupling (Fig. 4A). Depending on the handedness of the structure, the two circular polarization states result in SPPs that propagate radially toward the center of the circle (Fig. 4B) or outward (Fig. 4C). In case of unidirectional inward coupling, a high-intensity standing wave is formed within the circle, whereas the field intensity is minimal in the case of unidirectional outward coupling. LPL, as an equal superposition of left and right circularly polarized waves, results in SPPs propagating equally inward and outward (Fig. 4D). SPPs emanate from sections of the coupler oriented at all angles with respect to the incident polarization, demonstrating the polarization-invariant coupling efficiency for LPL. This feature becomes clear by comparing the properties of our structure with those of a ring-shaped groove (Fig. 4E), which is functionally equivalent to conventional SPP couplers. The NSOM image of the SPP field above the latter shows that SPPs can only be generated where the incident polarization is perpendicular to the groove (Fig. 4F).

Our couplers may form the basis for novel plasmonic devices and can be used to both improve efficiency and lower cross-talk in plasmonic networks. The possibility of encoding the polarization information in SPPs is particularly relevant based on recent evidence that SPPs preserve quantum coherence (*21*), which suggests that the structure may be used to reversibly convert polarization-encoded photon qubits to SPPs. This could help to further harness the unique properties of SPPs for applications in quantum information.

References and Notes

1. S. A. Maier, *Plamonics: Fundamentals and Applications* (Springer-Verlag, New York, 2007).
2. M. L. Juan, M. Righini, R. Quidant, *Nat. Photonics* **5**, 349 (2011).
3. S. Nie, S. R. Emory, *Science* **275**, 1102 (1997).
4. S. Kim *et al.*, *Nature* **453**, 757 (2008).
5. P. Genevet *et al.*, *Appl. Opt.* **50**, G56 (2011).
6. H. J. Lezec, J. A. Dionne, H. A. Atwater, *Science* **316**, 430 (2007).
7. T. Kosako, Y. Kadoya, H. F. Hofmann, *Nat. Photonics* **4**, 312 (2010).
8. N. Yu *et al.*, *Science* **334**, 333 (2011).
9. N. Yu, Q. Wang, F. Capasso, *Laser Photonics Rev.* **6**, 24 (2012).
10. E. Ozbay, *Science* **311**, 189 (2006).
11. M. L. Brongersma, V. M. Shalaev, *Science* **328**, 440 (2010).
12. H. A. Atwater, A. Polman, *Nat. Mater.* **9**, 205 (2010).
13. A. G. Curto *et al.*, *Science* **329**, 930 (2010).
14. F. López-Tejeira *et al.*, *Nat. Phys.* **3**, 324 (2007).
15. A. Baron *et al.*, *Nano Lett.* **11**, 4207 (2011).
16. Y. Liu *et al.*, *Nano Lett.* **12**, 4853 (2012).
17. T. Tanemura *et al.*, *Nano Lett.* **11**, 2693 (2011).
18. A. Archambault, T. V. Teperik, F. Marquier, J. J. Greffet, *Phys. Rev. B* **79**, 195414 (2009).
19. See supplementary materials on *Science* Online.
20. A. Yariv, P. Yeh, *Photonics: Optical Electronics in Modern Communications*; Oxford Series in Electrical and Computer Engineering (Oxford Univ. Press, New York, 2006).
21. G. Di Martino *et al.*, *Nano Lett.* **12**, 2504 (2012).

Acknowledgments: Part of this work was performed at the Center for Nanoscale Systems (CNS), a member of the National Nanotechnology Infrastructure Network (NNIN), which is supported by the NSF (under award ECS-0335765). CNS is part of Harvard University. This research is supported in part by the Air Force Office of Scientific Research under grant FA9550-12-1-0289. J.L. acknowledges the fellowship support from the Agency for Science, Technology and Research (A*STAR), Singapore. X.-C.Y. acknowledges the support given by the National Natural Science Foundation of China under grants 61036013 and 61138003, the Ministry of Science and Technology of China under grant 2009DFA52300 for China-Singapore collaborations, and the National Research Foundation of Singapore under grant NRF-G-CRP 2007-01. The authors express thanks to M. Kats (School of Engineering and Applied Sciences, Harvard University), K. A. C. Lee and Y. Zhou (Singapore Institute of Manufacturing Technology), and L. Du (Nanyang Technological University) for their assistance in the preparation of the manuscript. Data are available upon request.

Supplementary Materials

www.sciencemag.org/cgi/content/full/340/6130/331/DC1
Materials and Methods
Figs. S1 to S7
Table S1
References (*22*, *23*)

6 December 2012; accepted 27 February 2013
10.1126/science.1233746

External Quantum Efficiency Above 100% in a Singlet-Exciton-Fission–Based Organic Photovoltaic Cell

Daniel N. Congreve,* Jiye Lee,* Nicholas J. Thompson,* Eric Hontz, Shane R. Yost, Philip D. Reusswig, Matthias E. Bahlke, Sebastian Reineke, Troy Van Voorhis, Marc A. Baldo†

Singlet exciton fission transforms a molecular singlet excited state into two triplet states, each with half the energy of the original singlet. In solar cells, it could potentially double the photocurrent from high-energy photons. We demonstrate organic solar cells that exploit singlet exciton fission in pentacene to generate more than one electron per incident photon in a portion of the visible spectrum. Using a fullerene acceptor, a poly(3-hexylthiophene) exciton confinement layer, and a conventional optical trapping scheme, we show a peak external quantum efficiency of (109 ± 1)% at wavelength λ = 670 nanometers for a 15-nanometer-thick pentacene film. The corresponding internal quantum efficiency is (160 ± 10)%. Analysis of the magnetic field effect on photocurrent suggests that the triplet yield approaches 200% for pentacene films thicker than 5 nanometers.

Conventional solar cells generate one electron for each photon that is absorbed. The output voltage is defined by the bandgap, and solar cells waste any excess photon energy as heat. Summing the thermal loss over the solar spectrum yields the Shockley-Queisser efficiency limit of 34% for solar cells containing a single, optimized semiconductor junction (*1*).

Splitting excited states, or excitons, generated after the absorption of high-energy photons presents one pathway beyond the single junction efficiency limit. Instead of harvesting a single electron, several charges can be obtained by dissociating the child excitons. For example, so-called multiple exciton generation mechanisms have been used to produce an average of more than one electron from an ultraviolet photon with energy four times the bandgap (*2*).

Singlet exciton fission is a type of multiple exciton generation mechanism found in organic semiconductors (*3*, *4*). It is notable because spin conservation disallows the usual competing loss process: thermal relaxation of the high-energy exciton into a single low-energy exciton. In fission, the low-energy exciton is a dark state, inaccessible by a direct transition from either the high-energy exciton or the ground state. Only the evolution of the high-energy state into two dark excitons is spin-allowed. Consequently, prior studies have suggested that singlet fission can be efficient even in the visible spectrum, harnessing photons of just twice the energy of the child excitons (*5*–*10*).

There is a side effect of spin in singlet fission, however. The dark exciton controls the electrical properties of the cell. These are decoupled from

Energy Frontier Research Center for Excitonics, Massachusetts Institute of Technology, Cambridge, MA 02139, USA.

*These authors contributed equally to this work.
†Corresponding author. E-mail: baldo@mit.edu